NASA TECHNICAL NOTE

NASA TN D-5309

DATA-REDUCTION TECHNIQUE FOR DETERMINING RAPIDLY RISING HEATING RATES TO THERMALLY THICK WALLS

by James L. Dillon, Robert L. Wright, and G. Louis Smith

Langley Research Center

Langley Station, Hampton, Va.

NATIONAL AERONAUTICS AND SPACE ADMINISTRATION • WASHINGTON, D. C. • JULY 1969

DATA-REDUCTION TECHNIQUE FOR DETERMINING RAPIDLY RISING HEATING RATES TO THERMALLY THICK WALLS

By James L. Dillon, Robert L. Wright, and G. Louis Smith

Langley Research Center
Langley Station, Hampton, Va.

NATIONAL AERONAUTICS AND SPACE ADMINISTRATION

For sale by the Clearinghouse for Federal Scientific and Technical Information
Springfield, Virginia 22151 – CFSTI price $3.00

DATA-REDUCTION TECHNIQUE FOR DETERMINING RAPIDLY RISING HEATING RATES TO THERMALLY THICK WALLS

By James L. Dillon, Robert L. Wright,
and G. Louis Smith
Langley Research Center

SUMMARY

The integral method of determining aerodynamic heat flux from temperatures measured at four locations within a thermally thick wall has been analyzed for rapidly rising heating rates and large thermal as well as physical thicknesses. A restricted-exponential function has been developed for curve fitting the four values of $c_w(T)\frac{\partial T}{\partial t}$ through the wall (where c_w denotes specific heat of wall material; T, temperature; and t, time). The restricted-exponential function more accurately describes the variation of $c_w(T)\frac{\partial T}{\partial t}$ through the wall than the previously used polynomial curve fit and improves the accuracy of the integral heating method for determining rapidly rising heating rates to walls of large thermal thickness (large temperature gradients through the wall). Results are presented for simulated flight measurements for both smooth temperature data and scattered temperature data (standard deviation of 15° R, or 8.3° K) for two arrangements of sensor locations through the wall.

INTRODUCTION

The methods and techniques of analyzing telemetered instrument measurements are a vital part of a flight experiment. Free-flight experimental data are, by nature, very sensitive to the data-reduction technique utilized. This is due to the test time, sampling rates of the measurements, environmental variations throughout the test period, and many possible sources of inaccuracy in the telemetered data.

Numerous methods have been developed for determining experimental heating results when test conditions require thick-wall calorimeters. These methods are discussed in reference 1. However, only the methods of references 1 to 7 deal with the nonlinear heating problem involving temperature-dependent thermal properties of the wall. One of these, the integral method as applied in reference 2, has been used successfully in evaluating the heat flux to a thermally thick (0.508-cm-thick) heat shield of the Fire spacecraft

(refs. 2 and 3). The adaptation in reference 2 of the integral method for integrating $c_w \frac{\partial T}{\partial t}$ (where c_w denotes specific heat of the wall material; T, temperature; and t, time) through the wall to determine the heating rate incorporates a third-order polynomial expression to fit experimental values of $c_w \frac{\partial T}{\partial t}$ obtained from temperature measurements at four locations through the wall.

In the present paper an assessment of this adaptation for walls of greater physical and thermal thickness than the Fire heat shield and a rapidly rising heat flux indicated that the accuracy could be improved by incorporating a restricted-exponential function to fit the experimental values of $c_w \frac{\partial T}{\partial t}$ through the wall. Data are presented for two arrangements of thermocouple locations, with both smooth and randomly scattered temperature histories.

SYMBOLS

A_n	coefficients in temperature expression (where $n = 0, 1, 2, 3, 4, 5, 6$)
a_n	coefficients in exponential function defining $c_w \frac{\partial T}{\partial t}$ (where $n = 0, 1, 2, 3$)
c_w	specific heat of wall material
k	conductivity
l	wall thickness
q	heat flux (heating rate)
S	sum of the squares of the residuals
T	temperature
t	time
x	depth
ρ_w	material density

Subscript:

i	thermocouple location

ANALYSIS

Integral Method

For a nonablating, homogeneous wall with no heat losses from the back surface, the one-dimensional (no temperature gradient along the wall) heat flux to the front surface is equal to the rate of change of heat stored within the wall. The heat flux can be expressed by

$$q = \rho_w \int_0^l c_w(T)\frac{\partial T}{\partial t}\,dx \tag{1}$$

The integral method for solving equation (1) requires the definition of the gradient of $c_w(T)\frac{\partial T}{\partial t}$ through the wall and the integration of the area under the curve to produce the heat flux. The accuracy in determining heat flux by this method depends on the definition of this gradient (analytical curve fit).

Analytical model.- Evaluation of the integral for a very large temperature gradient through the wall was made by analytically simulating a flight heating-rate history and comparing the heating rates computed by the integral method with the simulated (known) heat input. The heating-rate history of figure 1 (typical of the side-wall heating on a slender-cone reentry vehicle at zero angle of attack) was applied in a direct thick-wall transient-heating program to a beryllium wall 1.524 cm thick. This program utilizes an explicit finite-difference computational technique to determine the temperatures within a wall for prescribed heating rates. Thermal measurement locations were assumed to be equally spaced within the wall at depths of 0.0254, 0.5080, 1.0160, and 1.5176 cm from the heated surface. The thermophysical properties of beryllium shown in figure 2 were used in the investigation. A detailed description of the thick-wall heating program may be found in the appendix to reference 1.

The accuracy of the temperatures computed by this program is dependent upon the size of the time interval used in the computations and the number of elements into which the wall is divided. An accuracy analysis of the thick-wall program for a 1.524-cm-thick wall divided into 11, 30, and 70 elements and for a 0.05-second time interval is presented in reference 1. For the heating-rate input of figure 1, a time interval of 0.05 second, and a wall division of 30 elements, as used in these computations, the temperatures at each location in the wall are estimated to be accurate within ±1 percent. The temperature histories for the four assumed measurement locations are shown in figure 1.

Polynomial curve fit.- The technique (developed in ref. 2) for evaluating the integral of equation (1) requires temperature histories at four thermocouple locations in the wall. One of these locations is as near to the heated surface as possible, and another at the

inside surface; the other two are equally spaced in the wall. The temperature history for each location (denoted by subscript i) is fitted with a sixth-order polynomial using the Chebyshev technique:

$$T_i(t) = A_{0,i} + A_{1,i}t + \ldots + A_{6,i}t^6 \tag{2}$$

where $i = 1, 2, 3, 4$.

For any selected instant of time, the temperature derivatives with respect to time $\frac{\partial T}{\partial t}$ are determined from the sixth-order polynomial, and the specific heat of the material c_w is obtained as a function of temperature for each thermocouple location. The distribution through the wall of the product $c_w(T)\frac{\partial T}{\partial t}$ (defined by the four locations in the wall) is then fitted with a third-order polynomial. The polynomial curve is analytically integrated (in closed form) from the heated surface to the inside surface and multiplied by the density of the material to yield the rate of change of stored heat in equation (1).

Temperature histories (fig. 1), simulating measurements from a flight experiment, were utilized in the integral method from reference 2 to compute heating rates for comparison with the exact heating-rate input of figure 1. Since no errors of data scatter were introduced, the comparison of the simulated and computed heating rate, presented in figure 3, provides an assessment of the accuracy of the data-reduction method. The computed heating rates are consistently higher than the simulated heating rates. Although the agreement is reasonably good at the lower heating rates, the accuracy of the method of reference 2 is noted to deteriorate for very large temperature gradients through the wall (higher heating rates).

The cause of the inaccuracy was investigated and was determined to be the shape of the analytical curve used to fit the values of $c_w \frac{\partial T}{\partial t}$ through the wall. Figure 4 presents the variation through the wall of $c_w \frac{\partial T}{\partial t}$ at three intervals of time. The symbols indicate the simulated experimental values of $c_w \frac{\partial T}{\partial t}$ at the four measurement locations which were obtained by differentiating the sixth-order polynomials fitted to the temperature histories and multiplying by the appropriate value of $c_w(T)$. The symbols are in excellent agreement with the solid line which shows the "actual" distribution of $c_w \frac{\partial T}{\partial t}$ through the skin, as provided by the direct computation of interior wall temperatures for the exact heating rate. At the early time ($t \approx 2$ seconds), the third-order polynomial which is fitted to the four simulated experimental data points provides adequate agreement. At the later times ($t \approx 6$ and 7 seconds) when the heating rate is rising rapidly, the shape of the third-order-polynomial curve differs significantly from the actual distribution, so that the integrated areas under the curves, and hence the heating rates, do not agree, as indicated in figure 3.

Exponential curve fit. - Since the accuracy of heating rates computed by the integral method of reference 2 is dependent on the curve fit of the four measured values of $c_w \frac{\partial T}{\partial t}$, numerous analytical expressions (polynomials and exponentials of various order) were systematically investigated to find a method which would define the distribution of $c_w \frac{\partial T}{\partial t}$ through the wall more accurately than does a third-order polynomial. Of the expressions investigated, an expression of the form

$$c_w \frac{\partial T}{\partial t} = e^{a_0+a_1x+a_2x^2+a_3x^3} \tag{3}$$

was found to provide the most accurate definition of the gradient of $c_w \frac{\partial T}{\partial t}$. Figure 5 shows the curve fit of the four simulated points obtained with the exponential function. Comparison with figure 4 shows that the exponential-function curve more closely approximates the shape of the actual curve than does the third-order polynomial.

Equation (3) cannot be integrated in closed form; therefore, the Gaussian technique of numerical integration was used to evaluate the integral $c_w \frac{\partial T}{\partial t} dx$ for the exponential curve fit, and the heating rate was computed from equation (1). The heating-rate history computed from the integrated exponential expression is presented in figure 6 along with the simulated heating rate and the heating rate computed by the method of reference 2 (third-order-polynomial curve fit). Agreement between the heating rate computed from the integrated exponential expression and the simulated heating rate is found to be within 2 percent at the highest heating rate.

Although the exponential expression produces more accurate representation of heating data, it does not correctly represent the variation of $c_w \frac{\partial T}{\partial t}$ through the wall. Figure 5 shows an inflection in the $c_w \frac{\partial T}{\partial t}$ curve when, in fact, the curve should have no points of inflection. (Very pronounced inflection points can result when experimental scatter is assumed in the four simulated values of $c_w \frac{\partial T}{\partial t}$.) Also, since heat losses from the back wall are assumed to be negligible, the gradient of $c_w \frac{\partial T}{\partial t}$ with x should be zero at the inside surface. To satisfy these requirements, a procedure was developed for determining the restricted third-order exponential function with a least-squares fit to the four values of $c_w \frac{\partial T}{\partial t}$. The restrictions are that its x derivative be zero at the inside surface and that there be no change in the sign of its second x derivative through the wall (no inflection point). The development of the method (hereinafter called the restricted-exponential method) is presented in the appendix. Results obtained with this restricted-exponential method were investigated for the more realistic conditions considered in the following section.

Data Scatter and Sensor Spacing

Data from free-flight experiments inherently possess some degree of scatter as a result of random inaccuracies in the telemetry and data readout systems. Also, the

location of the thermal sensors in the wall may differ from flight test to flight test. The sensitivity of the restricted-exponential method to these factors was investigated for a 1.524-cm-thick beryllium wall.

Effect of data scatter.- Scattered data (simulated flight temperature data) were generated by applying random scatter (produced by a random number generator) to the smooth temperature histories of figure 1. A standard deviation of 15° R (8.3° K) was used in the investigation. The scattered temperature data were fitted with sixth-order polynomials as outlined in the previous section and the derivative histories are shown in figure 7. Values of $c_W \frac{\partial T}{\partial t}$ at each measurement location were determined and are shown by the symbols in figure 8 for $t = 2$, 6, and 7 seconds. Also shown is the actual distribution of $c_W \frac{\partial T}{\partial t}$ through the wall at these three times, as in figures 4 and 5. The simulated data do not lie on the actual distribution curve, because they were derived from a fairing of scattered temperature data. The restricted-exponential least-squares fit of the points is a better representation of the actual distribution than is the third-order-polynomial curve fit.

Integration of the $c_W \frac{\partial T}{\partial t}$ distributions derived from the scattered temperature data produced the heating-rate data of figure 9 for a 1.524-cm-thick beryllium wall. The restricted-exponential method improved the accuracy at the higher heating rates; however, for the lower heating rates ($q \approx 200$ to 400 Btu/ft^2-sec or 226.98 to 453.96 watts/cm^2), the restricted-exponential method was less accurate than the third-order-polynomial method of reference 2.

The heating rates computed by both methods oscillate about the simulated heating-rate history. These oscillations result from oscillations in the $\frac{\partial T}{\partial t}$ history obtained from the sixth-order-polynomial fit of the scattered temperature data. Figure 7 shows these oscillations in the $\frac{\partial T}{\partial t}$ history obtained from the scattered data. Since the four values of $c_W \frac{\partial T}{\partial t}$ define the curves which are integrated to obtain heating rates at specified times, the oscillations in $\frac{\partial T}{\partial t}$ directly produce the oscillations in the computed heating-rate history. Improved techniques to curve-fit the temperature histories may eliminate some of the oscillations and the resulting error in the heating data.

Effect of sensor spacing.- The number and location of thermal sensors in a thick-wall calorimeter vary from one flight test to the next, depending on the experimental requirements and the number of telemetry channels available. Project Fire (refs. 2 and 3) utilized four thermocouples equally spaced through the wall. To determine the effects of unequal sensor spacing on the accuracy of the restricted-exponential method, the 0.600-inch-thick (1.524-cm) beryllium model was analyzed with the two interior measurements closer to the heated surface. For the analysis, the two interior temperature measurements were located 0.100 and 0.300 inch (0.254 and 0.762 cm) from the heated

surface. Such an arrangement would more accurately detect the shape of the temperature profile through the wall.

Temperature data at each thermocouple location were obtained for the simulated heating history of figure 1. The scatter applied to the temperature at each thermocouple was identical with that applied to the temperatures at the equally spaced thermocouples in the previous section. The resulting data were fitted with the restricted-exponential expression and compared with the actual distribution and the third-order-polynomial method of reference 2. Figure 10 presents the $c_w \frac{\partial T}{\partial t}$ variation through the wall for the unequally spaced thermocouple arrangement. For both thermocouple arrangements, the restricted-exponential curves define the gradient through the wall more accurately than the third-order polynomial (figs. 10 and 8).

Heating rates are shown in figure 11 for the unequal thermocouple spacing. The restricted-exponential method produces heating rates in close agreement with the exact heat input at the highest heating rates. At the lower heating rates, the restricted-exponential method also produced more accurate results than the third-order polynomial, unlike the results of figure 9 for equal sensor spacing.

CONCLUSIONS

The integral method of determining heating rates from temperatures measured at four locations within a thermally thick wall has been analyzed for rapidly rising heating rates and large thermal as well as physical thicknesses. An exponential function with two restrictions has been developed to curve-fit the measured values of $c_w(T)\frac{\partial T}{\partial t}$ (where c_w denotes specific heat of wall material; T, temperature; and t, time) and describe its variation through the wall. The restricted-exponential method has been analyzed for a 1.524-cm-thick beryllium wall with smooth and scattered data and for two sensor spacing arrangements. The following conclusions are noted:

1. The restricted-exponential method provides a better representation of the $c_w \frac{\partial T}{\partial t}$ distribution through the wall than the previously used polynomial curve fit.

2. With data scatter (standard deviation of 15° R, or 8.3° K) and equal sensor spacing, the restricted exponential method is more accurate than the polynomial method at higher heating rates but less accurate at lower heating rates.

3. The restricted-exponential method is more accurate than the polynomial method for both high and low heating rates for scattered data and unequal sensor spacing (interior sensors installed close to the heated surface to detect the slope of the temperature profile through the wall more accurately).

Langley Research Center,
National Aeronautics and Space Administration,
Langley Station, Hampton, Va., April 24, 1969,
711-02-09-01-23.

APPENDIX

OPTIMAL FIT OF THIRD-ORDER EXPONENTIAL FUNCTION TO DATA

A method of obtaining an optimal fit (in the sense of least squares) of the third-order exponential $c_w \frac{\partial T}{\partial t} = e^{a_0+a_1x+a_2x^2+a_3x^3}$, subject to constraints, to a set of data is presented. In order to satisfy the conditions that the $c_w \frac{\partial T}{\partial t}$ variation with x should have no inflection points and have a zero slope at the inside wall, the following constraints have been imposed on the exponential curve fit:

$$\frac{\partial y}{\partial z} = 0 \quad \text{at} \quad z = 0 \tag{A1}$$

$$\frac{\partial^2 y}{\partial z^2} \geqq 0 \quad \text{for all} \quad z \quad \text{on} \quad [0,l] \tag{A2}$$

where

$$z = l - x \tag{A3}$$

and

$$y = \log_e c_w \frac{\partial T}{\partial t} = a_0 + a_1 z + a_2 z^2 + a_3 z^3 \tag{A4}$$

Expression (A2) is used in place of $\frac{\partial^2}{\partial z^2}\left(c_w \frac{\partial T}{\partial t}\right) \geqq 0$, which is the direct requirement that there be no inflection points in the $c_w \frac{\partial T}{\partial t}$ curve, in order to make the procedure more tractable. Neglecting gradients of c_w yields

$$\frac{\partial^2 y}{\partial z^2} = \frac{\frac{\partial^2}{\partial z^2}\left(c_w \frac{\partial T}{\partial t}\right)}{c_w \frac{\partial T}{\partial t}} - \left[\frac{\frac{\partial}{\partial z}\left(c_w \frac{\partial T}{\partial t}\right)}{c_w \frac{\partial T}{\partial t}}\right]^2$$

The last term on the right-hand side is positive because it is squared, and $\frac{\partial T}{\partial t}$ is positive so that the constraint $\frac{\partial^2 y}{\partial z^2} \geqq 0$ requires that $\frac{\partial^2}{\partial z^2}\left(c_w \frac{\partial T}{\partial t}\right) \geqq 0$. It is noted that the solution developed herein for an optimal third-order-exponential curve fit will not represent the best fit for a quartic exponential.

APPENDIX

The condition of equation (A1) is easily satisfied by setting

$$a_1 = 0 \tag{A5}$$

which is the reason for introducing z by equation (A3). Then from equation (A4),

$$\frac{\partial^2 y}{\partial z^2} = 2a_2 + 6a_3 z$$

Thus, the inequality (A2) may be rewritten as

$$a_2 \geqq 0 \tag{A6a}$$

$$2a_2 + 6a_3 l \geqq 0 \tag{A6b}$$

In the usual manner of the method of least squares, the sum of the squares of the residuals S is formed (ref. 8):

$$S = \sum_{i=1}^{n} \left(a_0 + a_2 z_i^2 + a_3 z_i^3 - y_i \right)^2 \tag{A7}$$

where z_i is the location of the temperature measurements and y_i is the measured value at the corresponding ith locations.

The problem is reduced to finding a set of values for a_0, a_2, and a_3 that satisfy the inequalities (A6) and minimizing S. The sum of the squares of the residuals S may easily be written as a quadratic in a_0, a_2, and a_3, so that the problem is one of quadratic programing (ref. 9). However, the present problem is sufficiently simple to obviate the elegant methods of quadratic programing.

The first step of the procedure is to minimize S with respect to a_0, a_2, and a_3. Consequently,

$$\frac{\partial S}{\partial a_0} = \frac{\partial S}{\partial a_2} = \frac{\partial S}{\partial a_3} = 0 \tag{A8}$$

Generating the partial derivatives of equation (A8) from equation (A7) and setting them equal to 0 produces

$$na_0 + \left(\sum_{i=1}^{n} z_i^2\right)a_2 + \left(\sum_{i=1}^{n} z_i^3\right)a_3 = \sum_{i=1}^{n} y_i \tag{A9a}$$

$$\left(\sum_{i=1}^{n} z_i^2\right)a_0 + \left(\sum_{i=1}^{n} z_i^4\right)a_2 + \left(\sum_{i=1}^{n} z_i^5\right)a_3 = \sum_{i=1}^{n} y_i z_i^2 \tag{A9b}$$

$$\left(\sum_{i=1}^{n} z_i^3\right)a_0 + \left(\sum_{i=1}^{n} z_i^5\right)a_2 + \left(\sum_{i=1}^{n} z_i^6\right)a_3 = \sum_{i=1}^{n} y_i z_i^3 \tag{A9c}$$

Equations (A9a) to (A9c) can be easily solved for a_0, a_2, and a_3 by the use of Cramer's rule. If the resulting values of a_0, a_2, and a_3 satisfy the inequalities (A6), the problem is solved.

If both inequalities (A6a) and (A6b) are violated, the data indicate a cubic for which $\frac{\partial^2 y}{\partial z^2} < 0$ over the entire interval. The best fit to these data which satisfies the inequalities (A6a) and (A6b) is simply

$$a_0 = \left(\sum_{i=1}^{n} y_i\right) \Big/ n$$

$$a_2 = a_3 = 0$$

However, it is unrealistic to attempt to fit a curve with positive curvature to data which are best fit by a curve with negative curvature throughout the region of interest, and this case is rejected.

In the case of $a_2 < 0$ but $2a_2 + 6a_3 l \geqq 0$, it is necessary to set $a_2 = 0$ and minimize S in equation (A7) with respect to a_0 and a_3. This leads to equations (A9a) and (A9c) with $a_2 = 0$. These two linear equations in two unknowns are then solved to give a_0 and a_3. If now $a_3 > 0$, these values of a_0, a_2 (=0), and a_3 constitute the solution. If $a_3 \leqq 0$, the case is rejected, since the data are again best fit by a curve with negative curvature throughout the region of interest.

Likewise, in the case of $a_2 \geqq 0$ but $2a_2 + 6a_3 l < 0$, it is necessary to set $2a_2 + 6a_3 l = 0$, which reduces to

$$a_3 = -\frac{a_2}{3\ell} \tag{A10}$$

Then, S is minimized with respect to a_0 and a_2, whereby the equation

$$\frac{\partial S}{\partial a_0} = \frac{\partial S}{\partial a_3} = 0$$

gives

$$na_0 + a_2 \sum_{i=1}^{n} \left(z_i^2 - \frac{z_i^3}{3\ell} \right) = \sum_{i=1}^{n} y_i \tag{A11a}$$

$$a_0 \sum_{i=1}^{n} \left(z_i^2 - \frac{z_i^3}{3\ell} \right) + a_2 \sum_{i=1}^{n} \left(z_i^2 - \frac{z_i^3}{3\ell} \right)^2 = \sum_{i=1}^{n} y_i \left(z_i^2 - \frac{z_i^3}{3\ell} \right) \tag{A11b}$$

Equations (A11) may be solved for a_0 and a_2, and a_3 is then computed from equation (A10). If $a_2 > 0$, the values of a_0, a_2, and a_3 are the acceptable solutions. However, if $a_2 \leq 0$, the case is rejected as before.

A schematic diagram of the procedure of fitting the third-order exponential to the data is presented in figure 12.

Proof that the foregoing procedure gives the best fit of the third-order exponential to the data under the given restraints can be given geometrically. As was previously noted, S is a quadratic in a_0, a_2, and a_3. In the a_0, a_2, a_3 space, S = Constant describes an ellipsoid which degenerates to a point for a_0, a_2, and a_3 equal to the best-fit values computed from equation (A8). At this point, $S = S_{min}$. For any S_1 and S_2 with $S_1 > S_2 > S_{min}$, the ellipsoid $S = S_2$ is entirely contained within the ellipsoid $S = S_1$, and any point on S_2 corresponds to a better fit to the data than any point on S_1.

Figure 13 shows the geometry in the a_2-a_3 plane. For clarity the a_0-dimension has been suppressed and the ellipsoids are shown as ellipses, but the discussion applies to the three-dimensional case. The planes $a_2 = 0$ and $2a_2 + 6a_3\ell = 0$ divide the space into four regions.

Region I is denoted as the set of points (a_0, a_2, a_3) for which the inequalities (A6) are satisfied, as indicated by point A. Region II is the set of points for which neither of the inequalities (A6) are satisfied, as shown by point B. Region III is the set of points for which

APPENDIX

$$a_2 < 0$$

$$2a_2 + 6a_3 l \geqq 0$$

as given by example points C, D, and E. Region IV is the set of points for which

$$a_2 \geqq 0$$

$$2a_2 + 6a_3 l < 0$$

as given by example points F and G.

If the solution of equations (A9) is in region I, it satisfies all requirements and is accepted. If the solution is in region II, the data are best fit by a cubic with completely negative curvature and the case is rejected because a least-squares fit with the constraints of positive curvature would be meaningless in application. If for the given data the solution of equations (A9) falls in region III, then equations (A9) do not apply. In this case, the (a_0, a_2, a_3) point for which S is a minimum and which satisfies the inequality (A6a) is the point of tangency of an ellipsoid which is tangent to the plane $a_2 = 0$, such as point C_1 in figure 13. This point is given by the solution to equations (A9a) and (A9c) with $a_2 = 0$. However, this $a_2 = 0$ point may fall on the boundary of region II, such as point D_1, where $a_3 \leqq 0$. In this event, the case is rejected.

Finally, as with point E, the smallest ellipsoid intersecting region I (touching region I at point E_1) may also intersect region II, so that although the given procedure gives a best fit satisfying all conditions (positive curvature throughout the interval), a better fit may be found with negative curvature throughout the interval. If the solution of equations (A9) lies in region IV, the same type of considerations apply as when the solution lies in region III.

REFERENCES

1. Howard, Floyd G.: Single-Thermocouple Method for Determining Heat Flux to a Thermally Thick Wall. NASA TN D-4737, 1968.

2. Cornette, Elden S.: Forebody Temperatures and Total Heating Rates Measured During Project Fire I Reentry at 38,000 Feet Per Second. NASA TM X-1120, 1965.

3. Cornette, Elden S.: Forebody Temperatures and Calorimeter Heating Rates Measured During Project Fire II Reentry at 11.35 Kilometers Per Second. NASA TM X-1305, 1966.

4. McDonough, John F.; and Youngbluth, Otto, Jr.: A Simple Method for Determining High Heat Rates by Using Slug Calorimeters. NASA TM X-1408, 1967.

5. Stroud, C. W.: A Numerical Method for Determining Heating Rates From Thick-Calorimeter Data. NASA TN D-3846, 1967.

6. Gaumer, G. R.; Parks, D. L.; and Kipp, H. W.: ASSET. Volume XIV – Heat Flux Calculation Procedures. Tech. Rep. AFFDL-TR-65-31, vol. XIV, U.S. Air Force, Apr. 1966. (Available from DDC as AD 480814.)

7. Powell, Walter B.; and Price, Theodore W.: A Method for the Determination of Local Heat Flux From Transient Temperature Measurements. ISA Trans., vol. 3, no. 3, July 1964, pp. 246-254.

8. Sokolnikoff, I. S.; and Redheffer, R. M.: Mathematics of Physics and Modern Engineering. McGraw-Hill Book Co., Inc. (New York), c.1958.

9. Boot, John C. G.: Quadratic Programming. Algorithms – Anomalies – Applications. Rand McNally & Co., 1964.

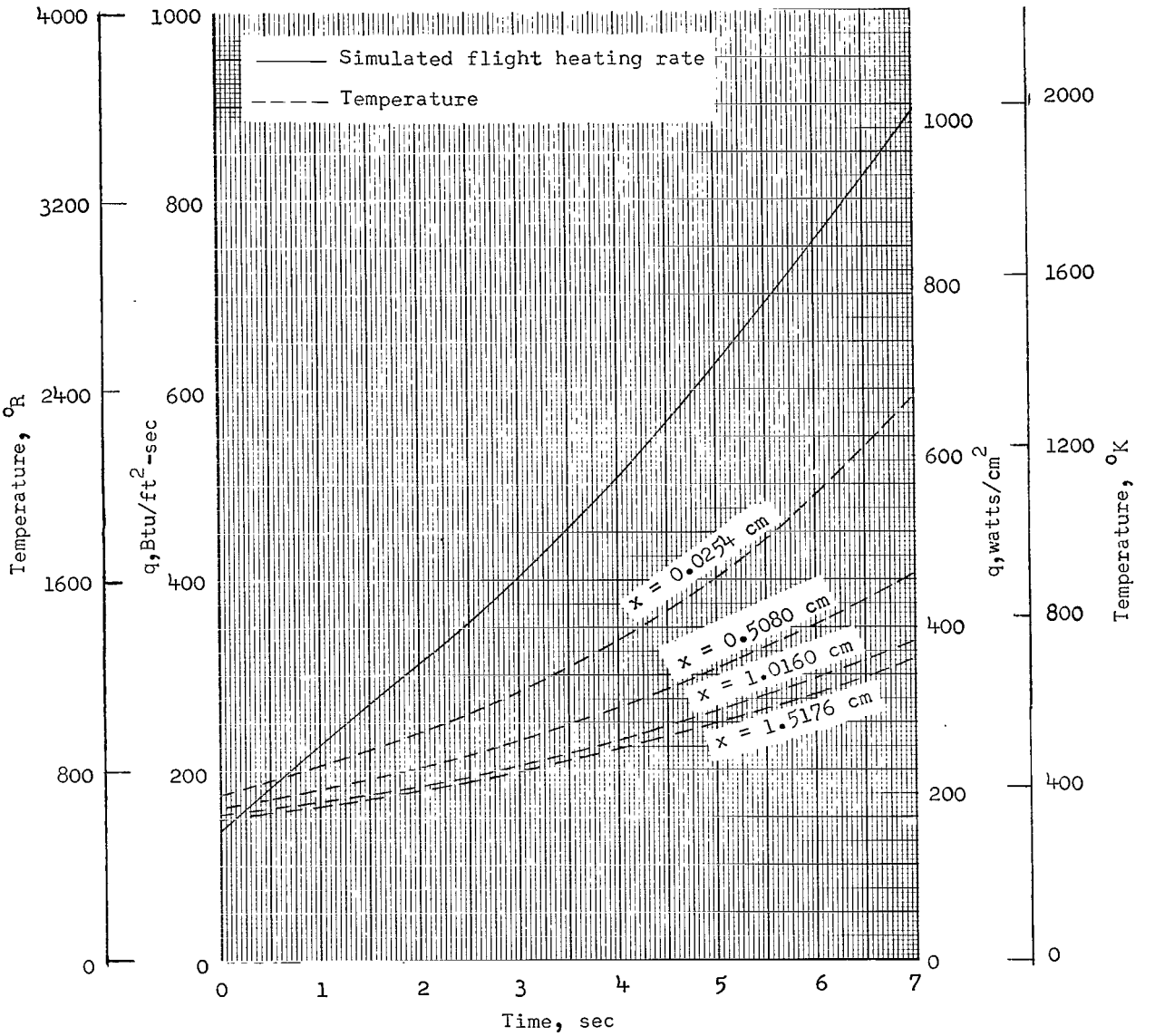

Figure 1.- Heating-rate history and associated temperature history at different locations in 1.524-cm-thick beryllium wall.

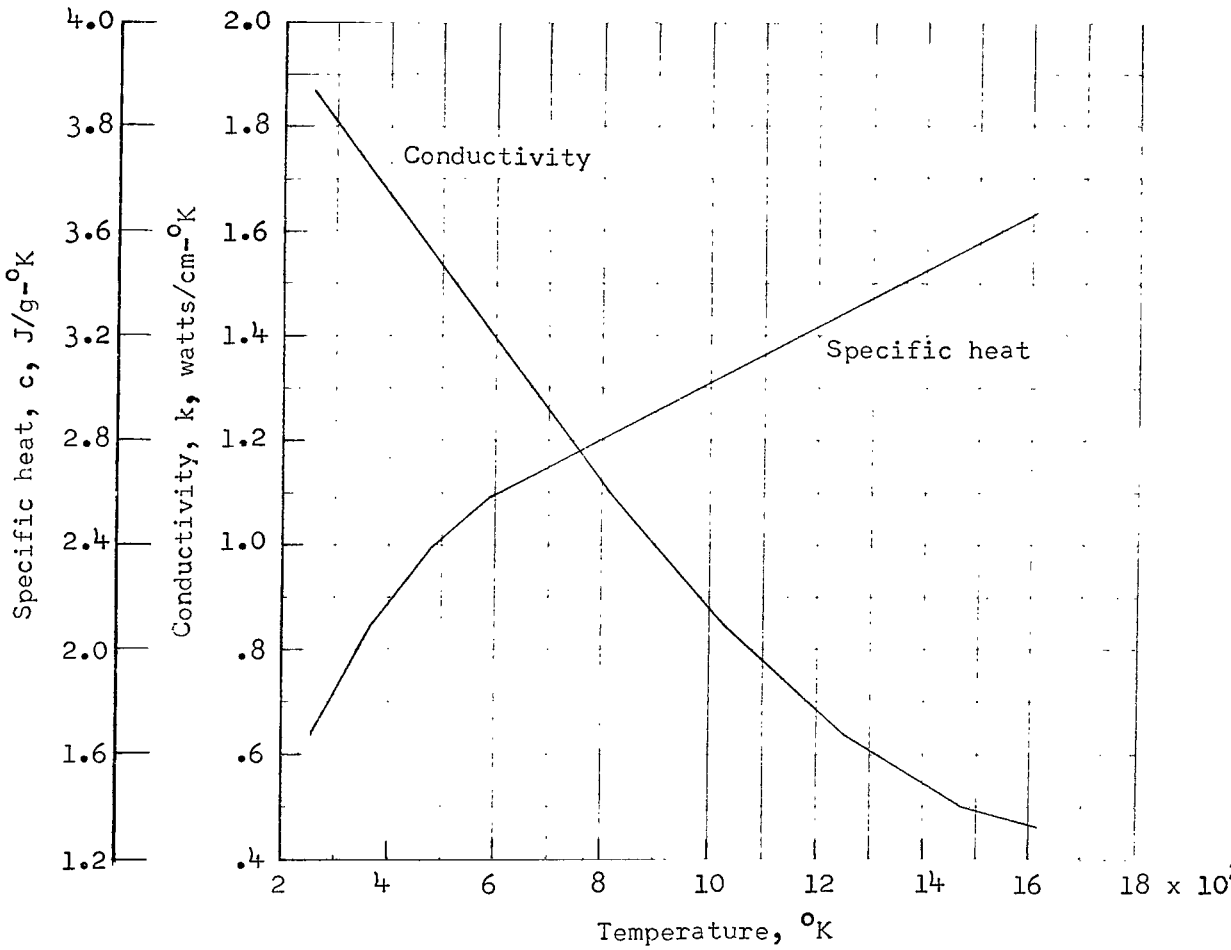

Figure 2.- Thermophysical properties of beryllium. Density, 1862.4 kg/m^3.

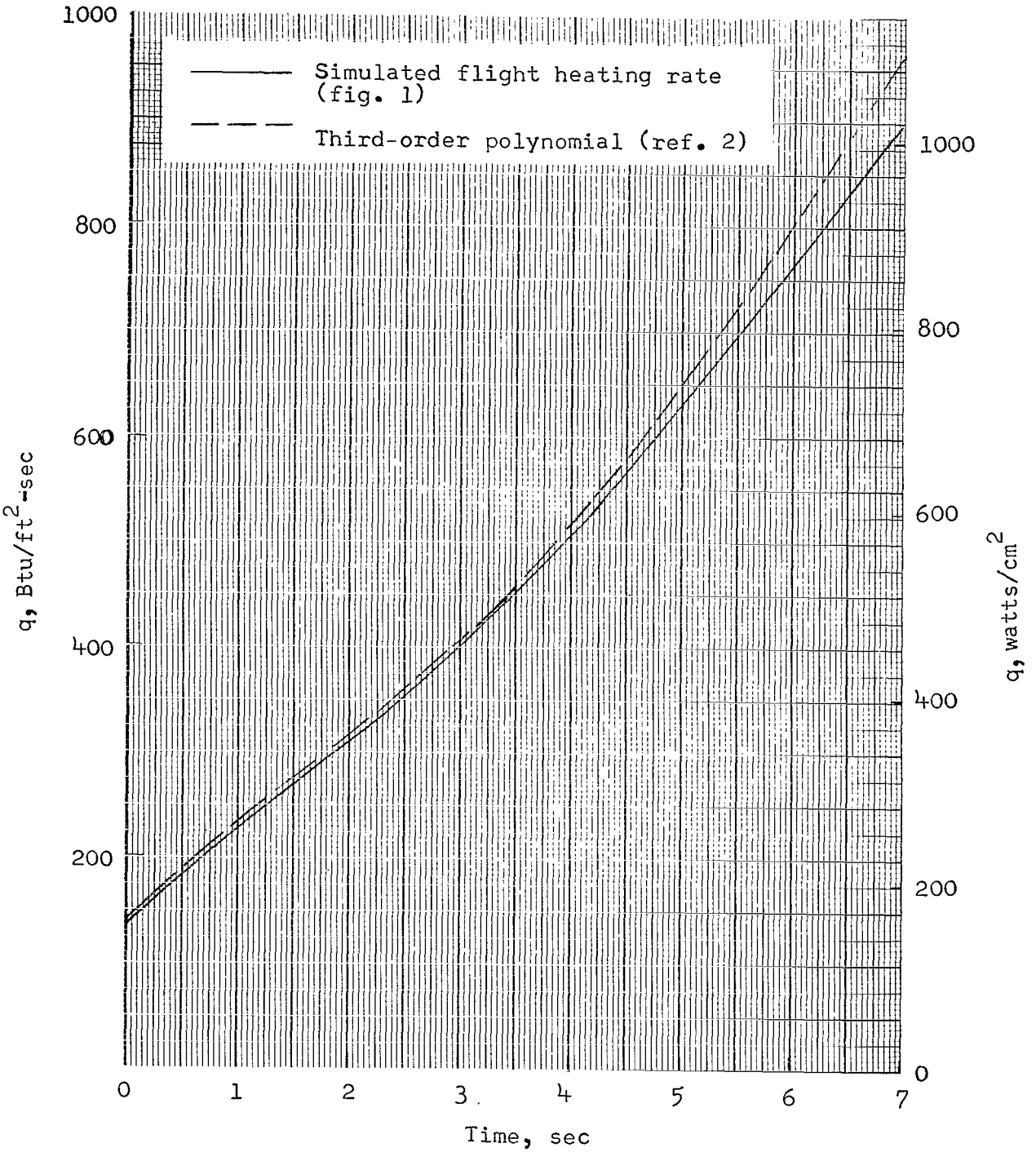

Figure 3.- Simulated heating rate and heating rate computed with third-order polynomial curve fit.

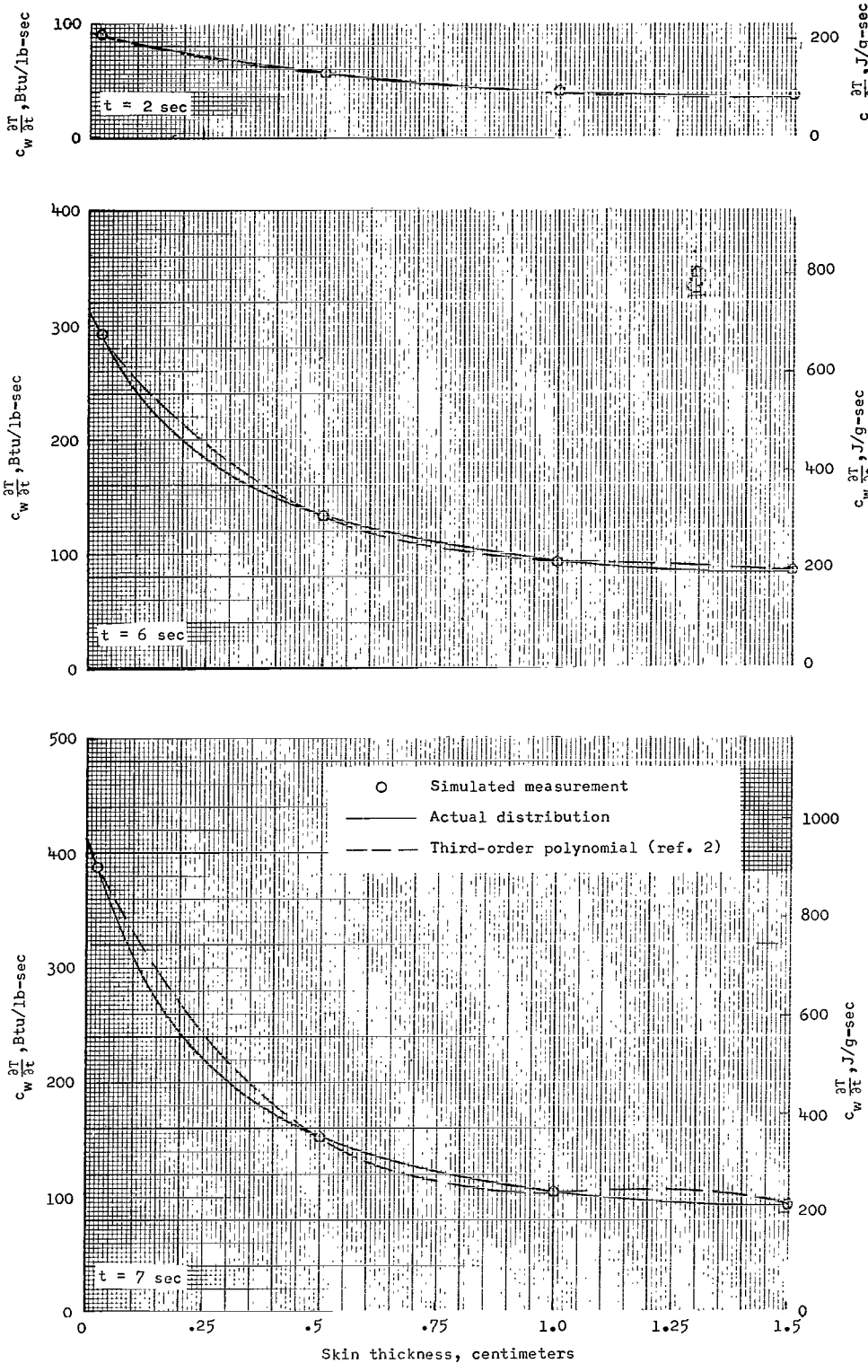

Figure 4.- Simulated data fitted analytically with third-order polynomial function (ref. 2).

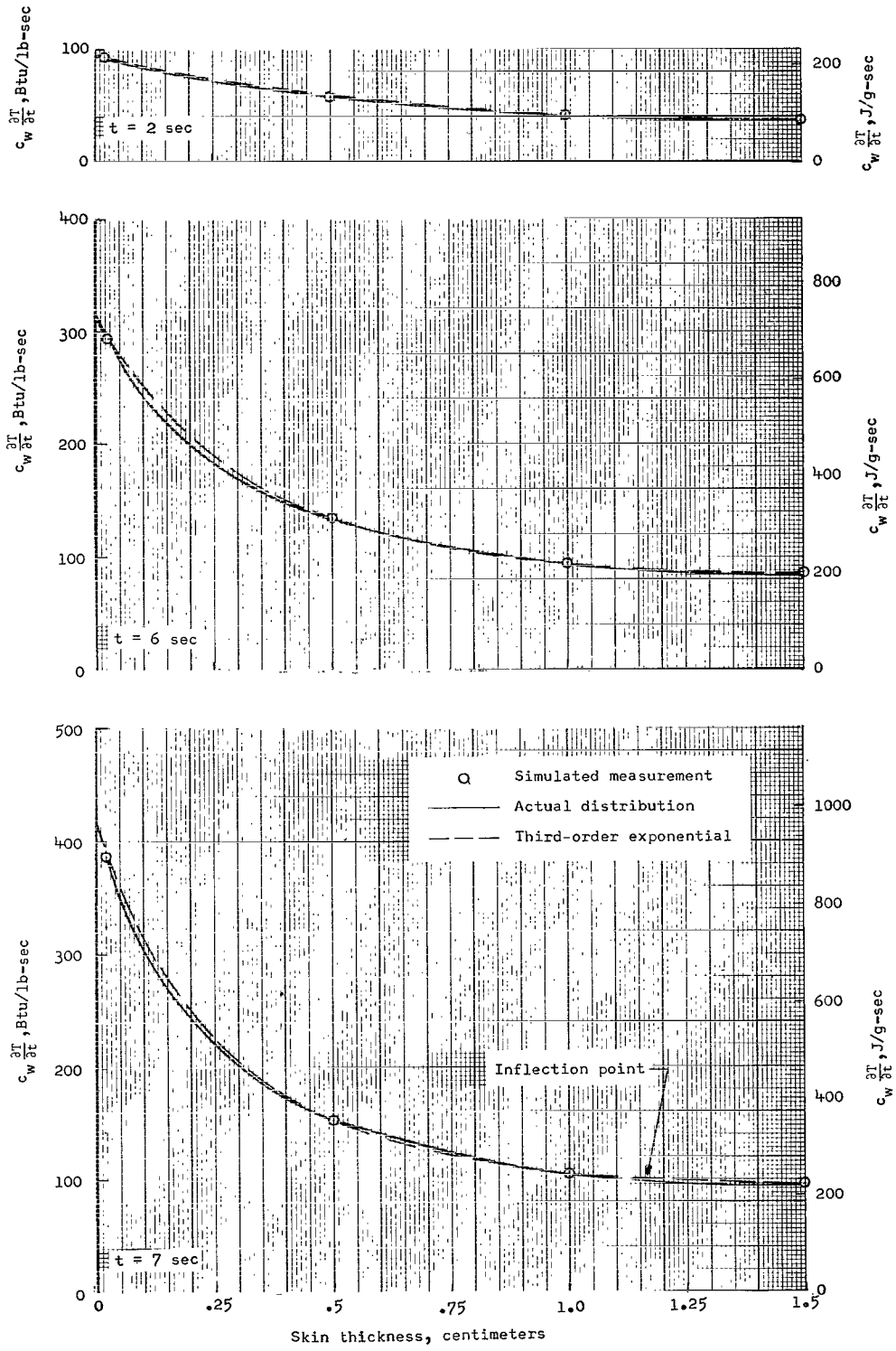

Figure 5.- Simulated data fitted analytically with third-order-exponential function.

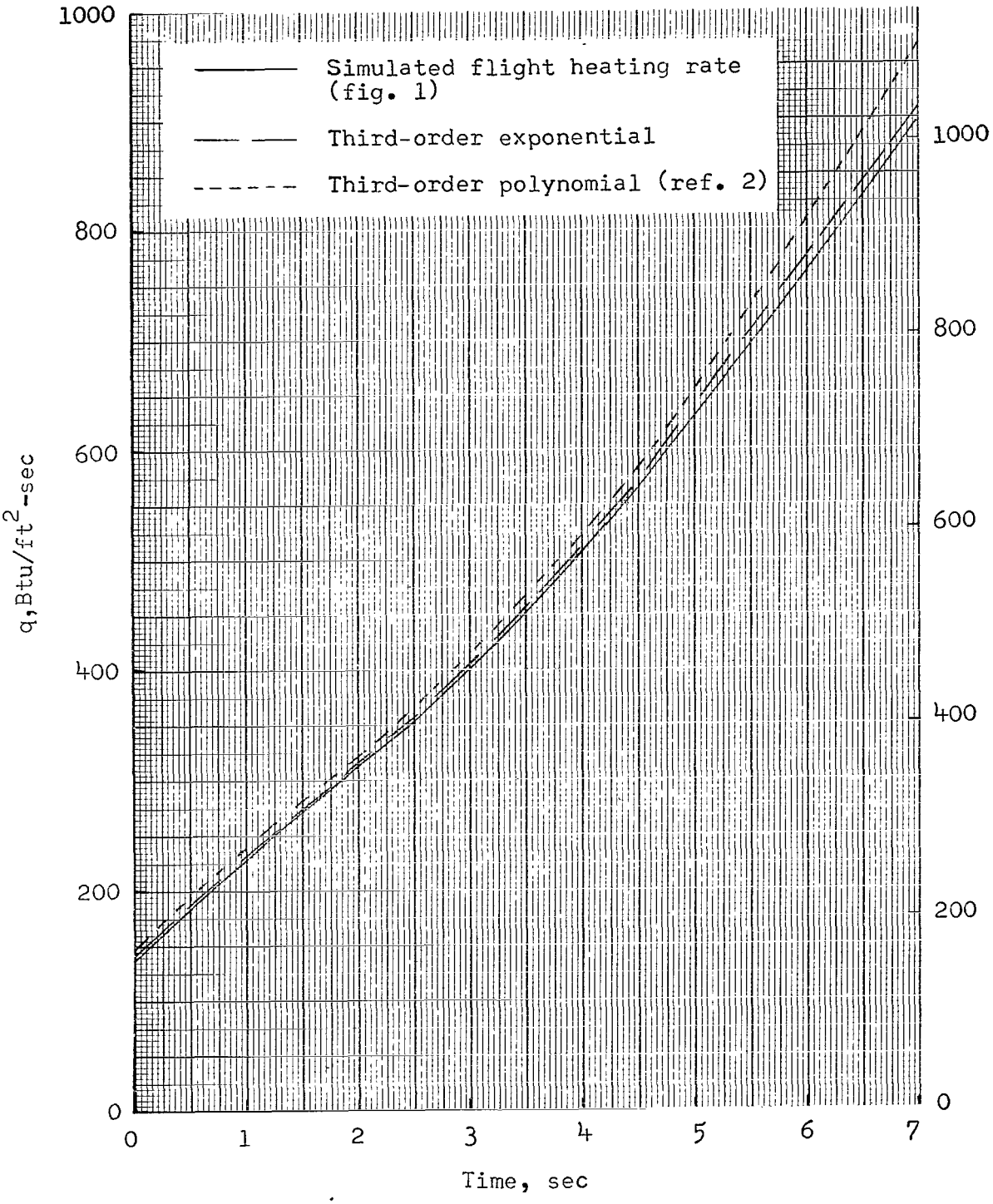

Figure 6.- Simulated heating rate and heating rates computed by integral method with third-order polynomial and third-order-exponential curve fits.

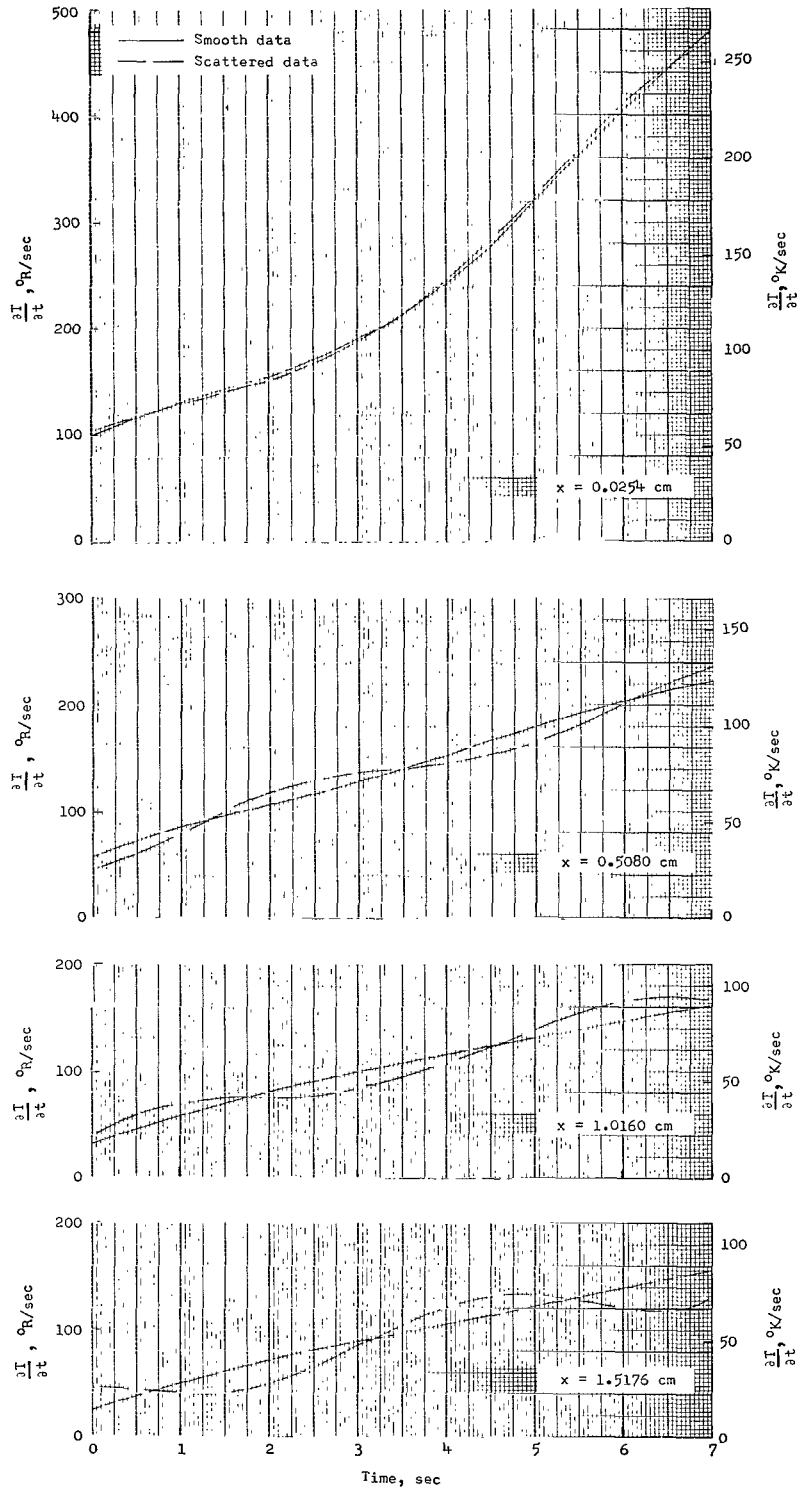

Figure 7.- Temperature-derivative histories (from sixth-order polynomial) for smooth and scattered data.

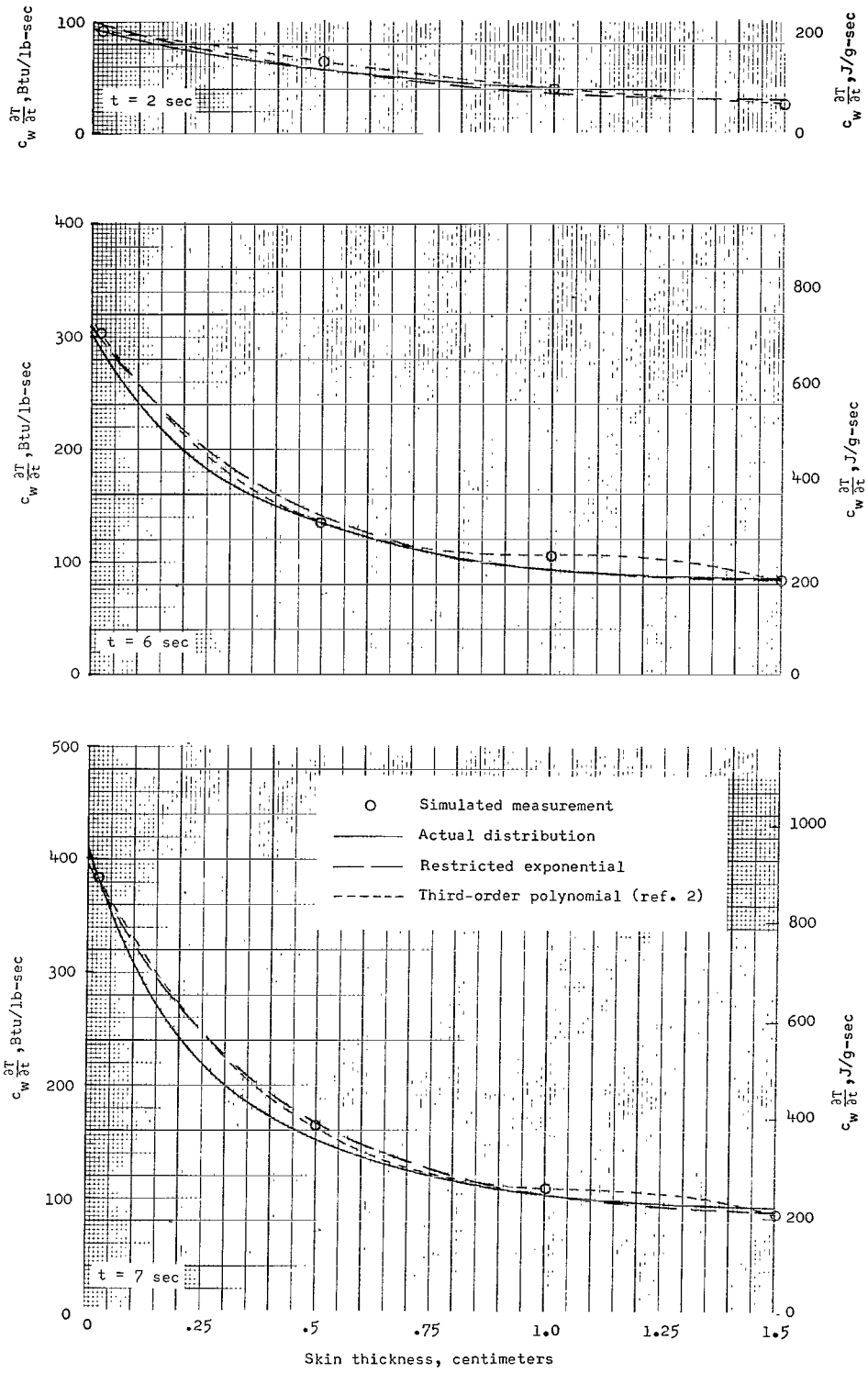

Figure 8.- Analytical fit of simulated data with data scatter.

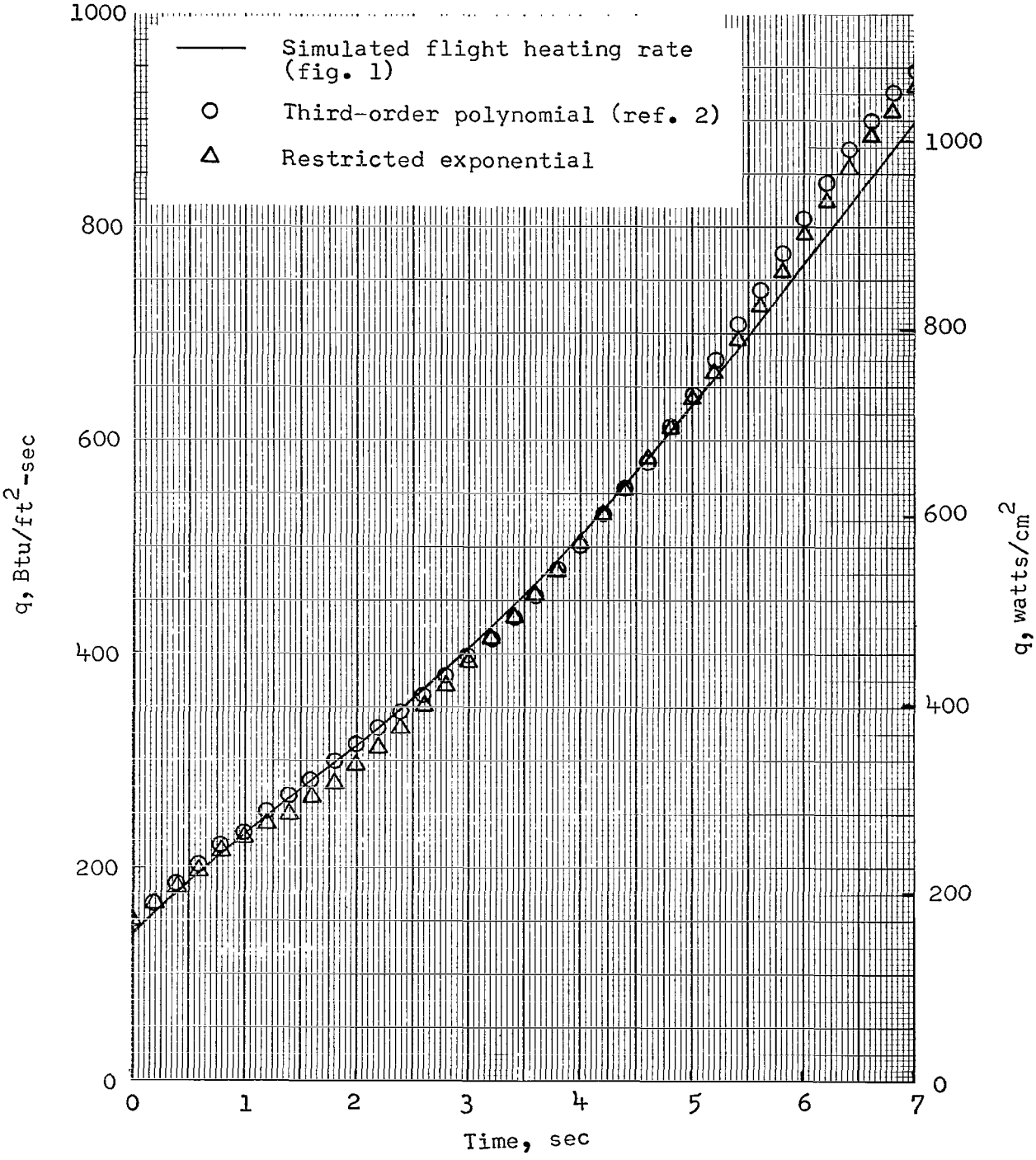

Figure 9.- Heating-rate histories with data scatter.

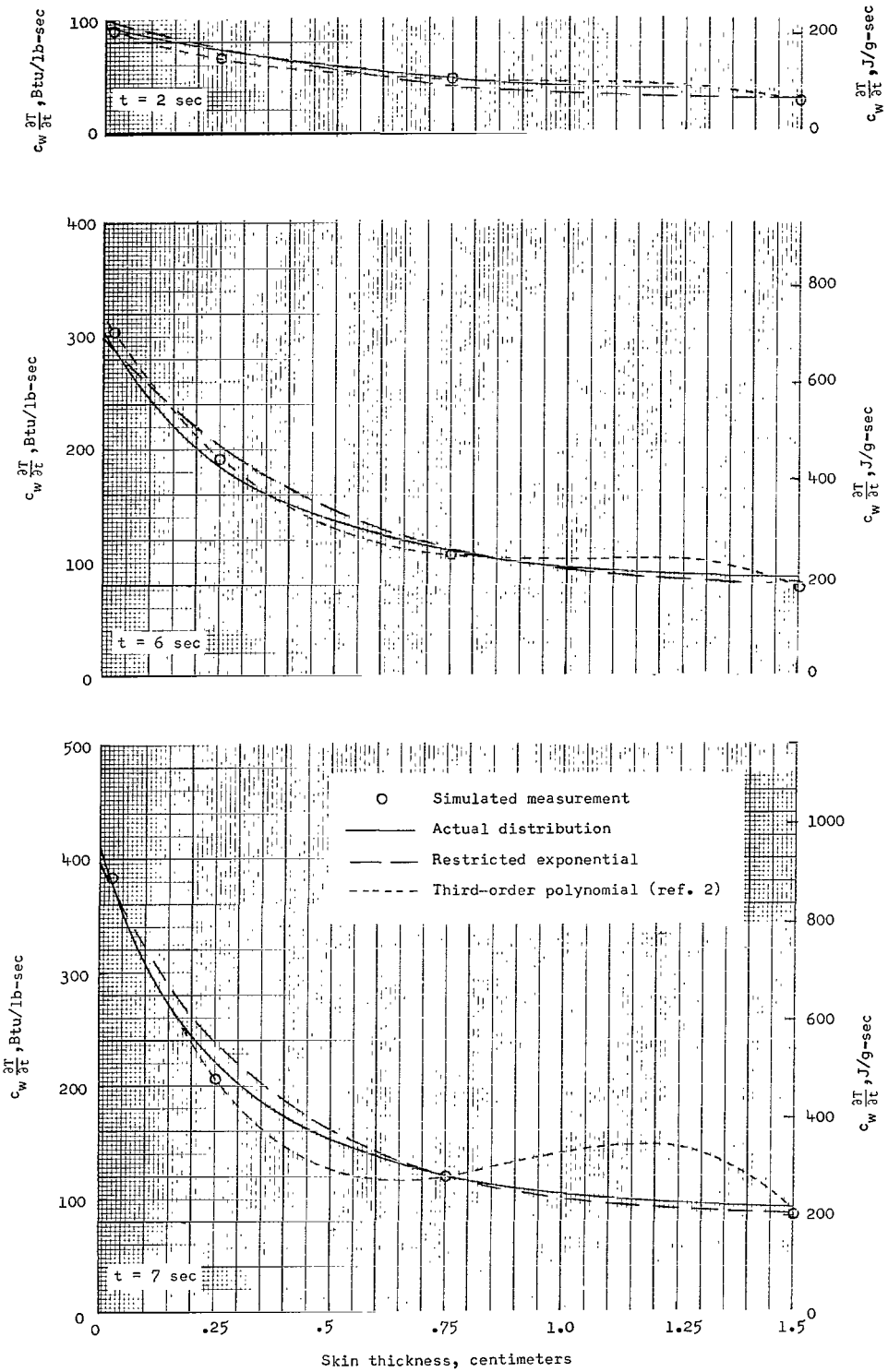

Figure 10.- Analytical fit of simulated data for unequal sensor spacing.

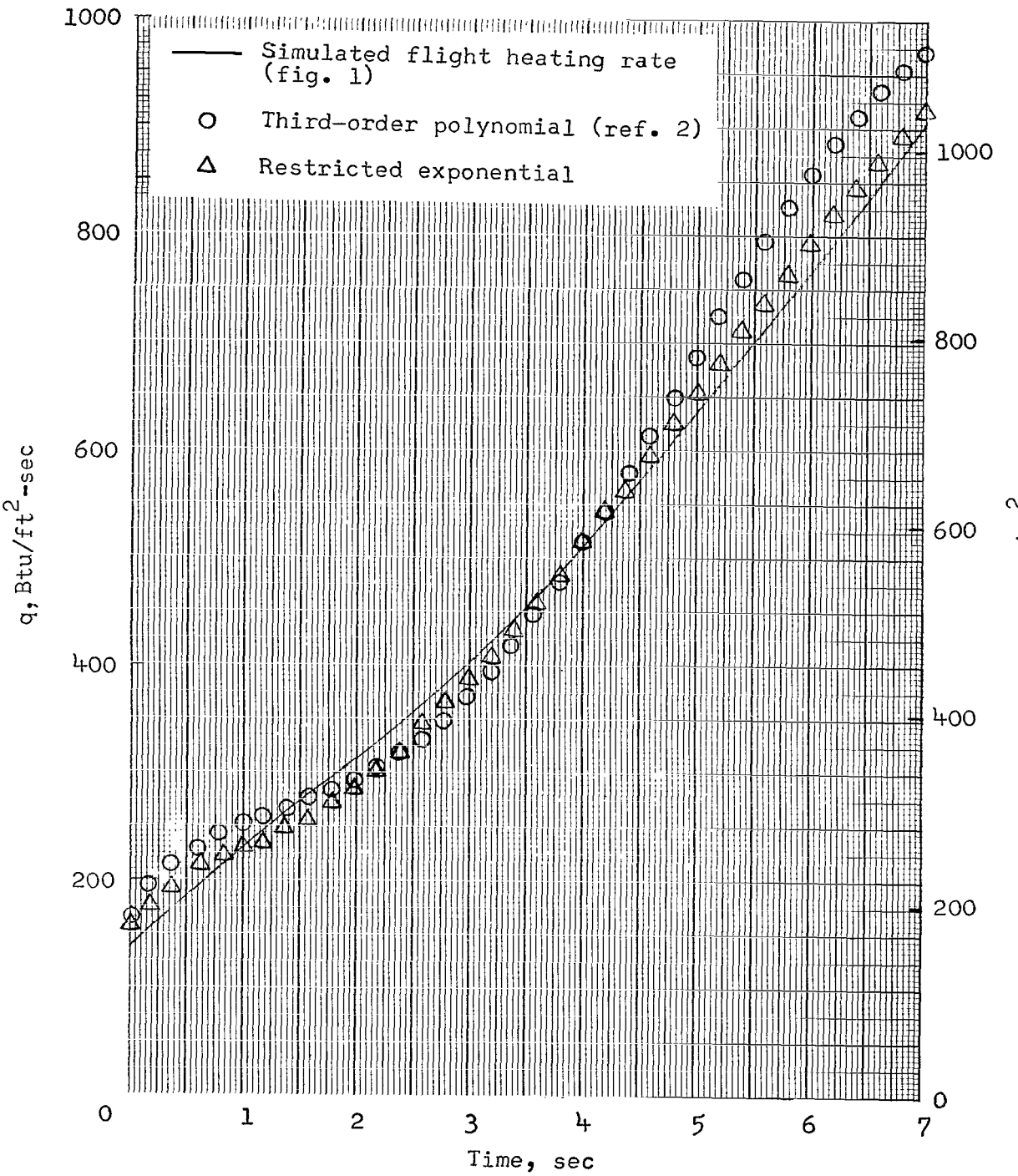

Figure 11.- Heating-rate histories for unequal sensor spacing.

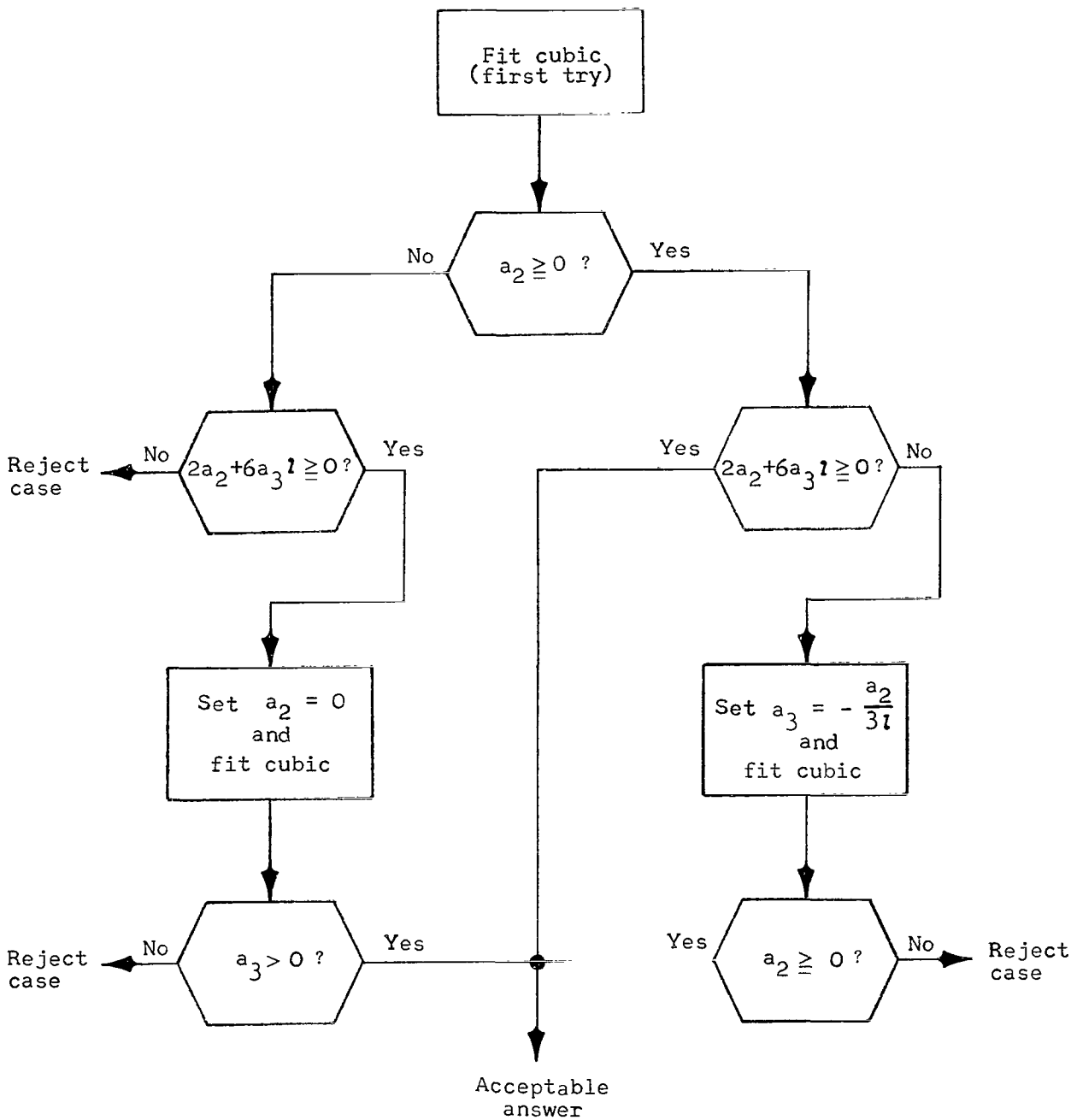

Figure 12.- Schematic diagram of procedure for fitting third-order exponential to data.

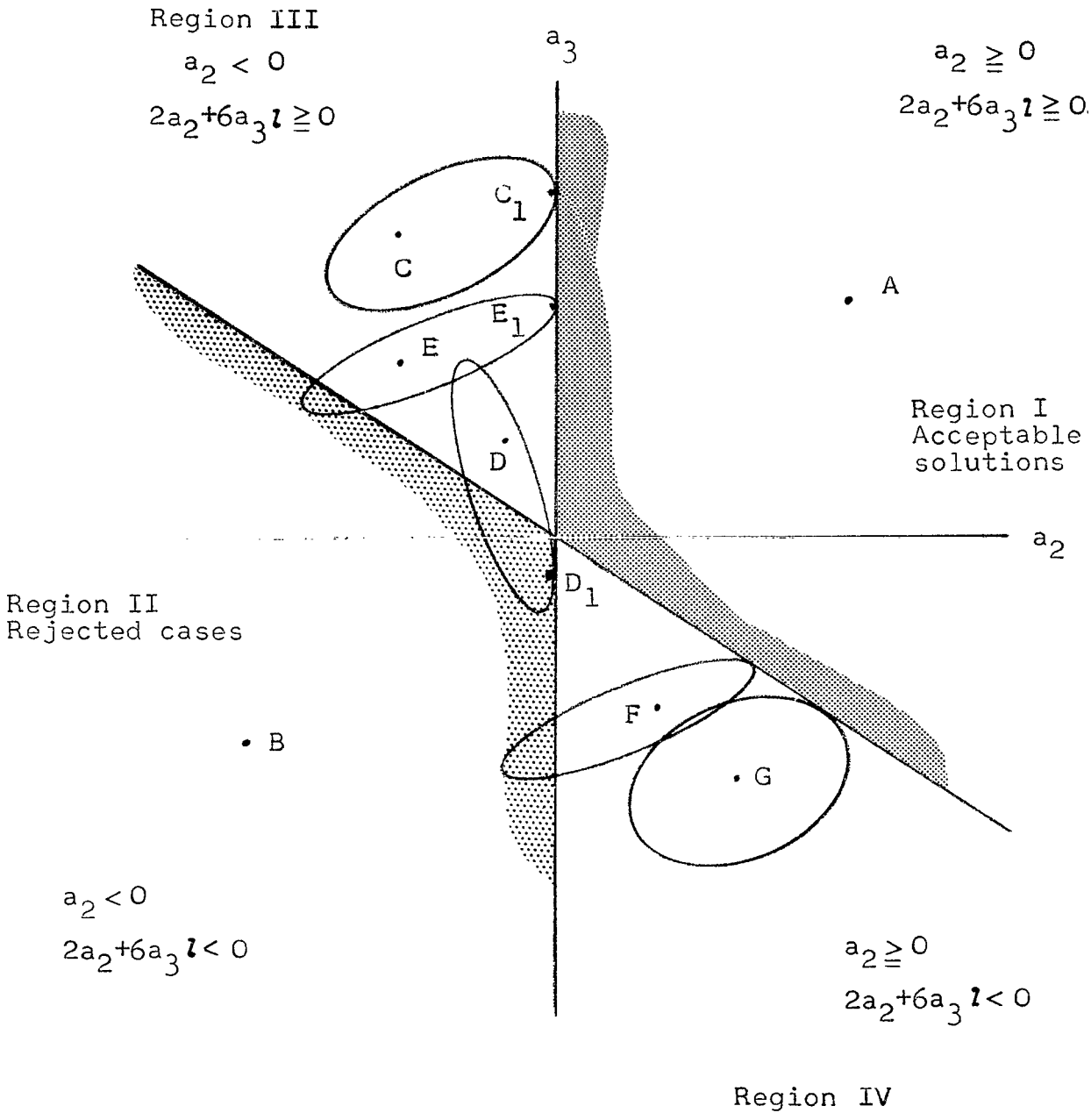

Figure 13.- Geometric interpretation of curve-fitting procedure.

"The aeronautical and space activities of the United States shall be conducted so as to contribute . . . to the expansion of human knowledge of phenomena in the atmosphere and space. The Administration shall provide for the widest practicable and appropriate dissemination of information concerning its activities and the results thereof."

—NATIONAL AERONAUTICS AND SPACE ACT OF 1958

NASA SCIENTIFIC AND TECHNICAL PUBLICATIONS

TECHNICAL REPORTS: Scientific and technical information considered important, complete, and a lasting contribution to existing knowledge.

TECHNICAL NOTES: Information less broad in scope but nevertheless of importance as a contribution to existing knowledge.

TECHNICAL MEMORANDUMS: Information receiving limited distribution because of preliminary data, security classification, or other reasons.

CONTRACTOR REPORTS: Scientific and technical information generated under a NASA contract or grant and considered an important contribution to existing knowledge.

TECHNICAL TRANSLATIONS: Information published in a foreign language considered to merit NASA distribution in English.

SPECIAL PUBLICATIONS: Information derived from or of value to NASA activities. Publications include conference proceedings, monographs, data compilations, handbooks, sourcebooks, and special bibliographies.

TECHNOLOGY UTILIZATION PUBLICATIONS: Information on technology used by NASA that may be of particular interest in commercial and other non-aerospace applications. Publications include Tech Briefs, Technology Utilization Reports and Notes, and Technology Surveys.

Details on the availability of these publications may be obtained from:

SCIENTIFIC AND TECHNICAL INFORMATION DIVISION

NATIONAL AERONAUTICS AND SPACE ADMINISTRATION

Washington, D.C. 20546